Electronic Supplementary Material (ESI) for Journal of Materials Chemistry C.

Supplementary Information

Achieving high energy density at low electric field of high-temperature sandwich-structured polymer dielectric composite by *β*-PVDF crystallinity regulation

Tianran Zhang[a], Qinzhao Sun[a], Zepeng Wang[a], Ruirui Kang[b], Fang Kang[a], Rong Xue[a], Jiping Wang[a*], and Lixue Zhang[a*]

a. State Key Laboratory for Mechanical Behavior of Materials, School of Materials Science and Engineering, Xi'an Jiaotong University, Xi'an, 710049, China.

b. Frontier Institute of Science and Technology, State Key Laboratory for Mechanical, Behavior of Materials, Xi'an Jiaotong University, Xi'an, 710049, China.

∗ Corresponding authors.

E-mail addresses: jpwang@mail.xjtu.edu.cn (Jiping Wang); lxzhang@mail.xjtu.edu.cn (Lixue Zhang)

Tel numbers: (86)-180 4907 6980 (Jiping Wang); (86)-18049076981 (Lixue Zhang)

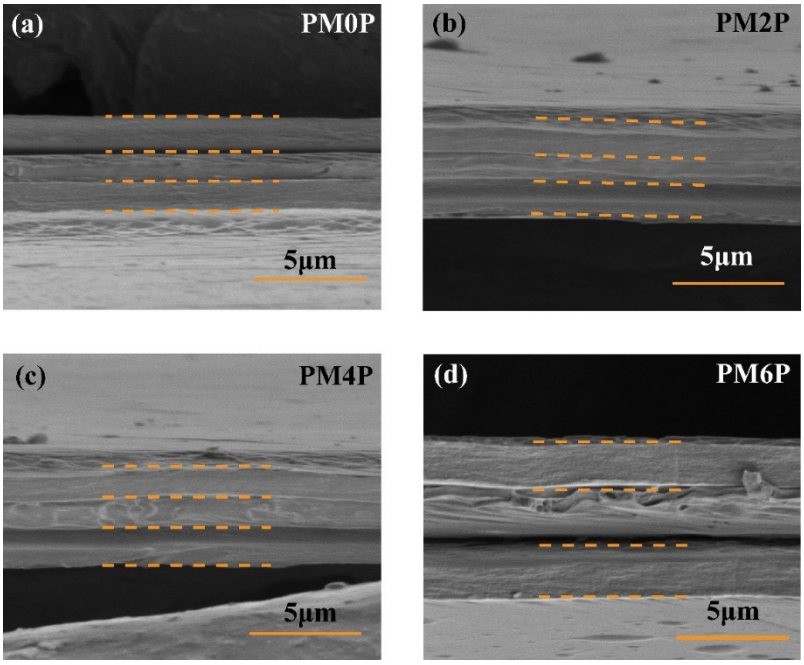

Figure S1 The cross-sectional SEM morphology of **(a)** PM0P, **(b)** PM2P, **(c)** PM4P and **(d)** PM6P.

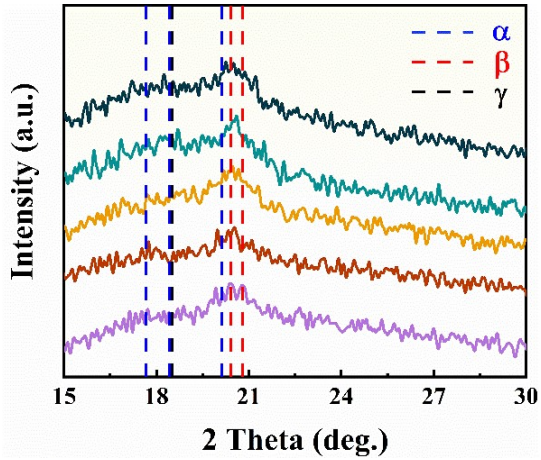

Figure S2 The XRD patterns for MO-x middle layer.

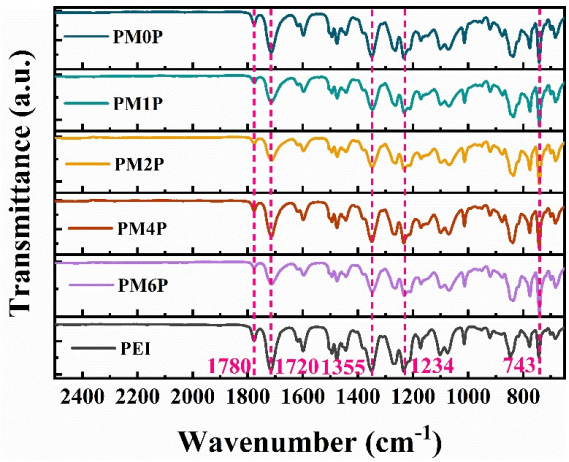

Figure S3 The FTIR spectra for sandwich-structured composites.

The FTIR spectra for sandwich-structured composites are shown in **Figure S3**. The bands at 1780 cm^{-1} and 1720 cm^{-1} are assigned to the imide group of PEI, and the bands at 1355 cm^{-1} and 743 cm^{-1} are associated with the C-N stretching and bending of PEI. The band at 1234 cm^{-1} is assigned aromatic ether for PEI. There is no significant change in FTIR spectra due to less MgO content in the whole sandwich-structured composites.

The crystallinity was calculated using the equation:

$$X(\%) = \frac{\Delta H_{exp}}{\Delta H^{\circ}} \times 100\% \quad \text{(S1)}$$

$$\Delta H_{exp} = \Delta H_{melt} - \Delta H_{cold\ cryst} \quad \text{(S2)}$$

where ΔH° is the heat fusion of 100% crystalline polymer, the value for PVDF is 104.7J/g. ΔH_{melt} is the experimental calculated melting enthalpy, $\Delta H_{cold\ cryst}$ is the experimental calculated cold crystalline enthalpy.

Table S1 ΔH_{exp} and crystallinity PMMA/PVDF blended composites with different MO contents.

MO (wt%)	ΔH_{exp} (J/g)	Crystallinity (%)
0	25.96	24.79%
1	31.05	29.66%
2	33.33	31.83%
4	31.29	29.89%
6	32.41	30.96%

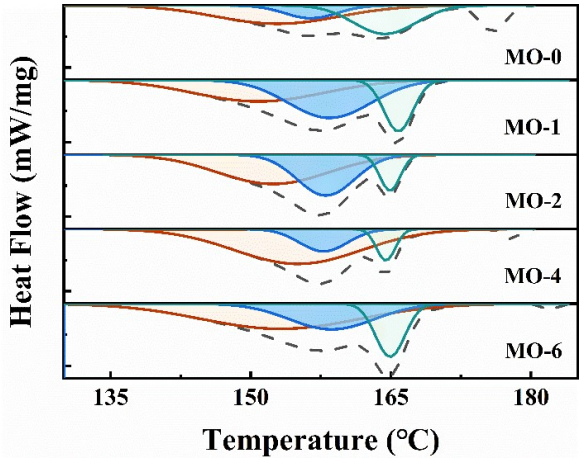

Figure S4 The deconvolution of the DSC thermographs of MO-x.

All the deconvoluted curves show the prominent melting peaks corresponding to α-, β- and γ-crystallization. The presence of the peak at around 165 °C is γ-phase (the green peaks in **Figure S4**). The peak at around 160 °C (the blue peaks in **Figure S4**) suggested β-phase and the side peak at around 155 °C (the orange peaks in **Figure S4**) suggested α phase crystallization[S1]. With the MO content increase, deconvoluted curves present the increasing in intensity and broadening of the β-phase peak, especially for MO-1 and MO-2, indicates gradually increasing of the β- phase crystallinity. The main reason for crystallization increasing is that the interaction between MgO nps and PVDF chains induce the all-trans conformation of the PVDF segments, then the all-trans conformation propagates during crystal growth. MgO nps also changes nucleation kinetics and acts as crystallization site in the process of promoting crystallization, increasing the number of spherulites and reducing the spherulites size [S2].

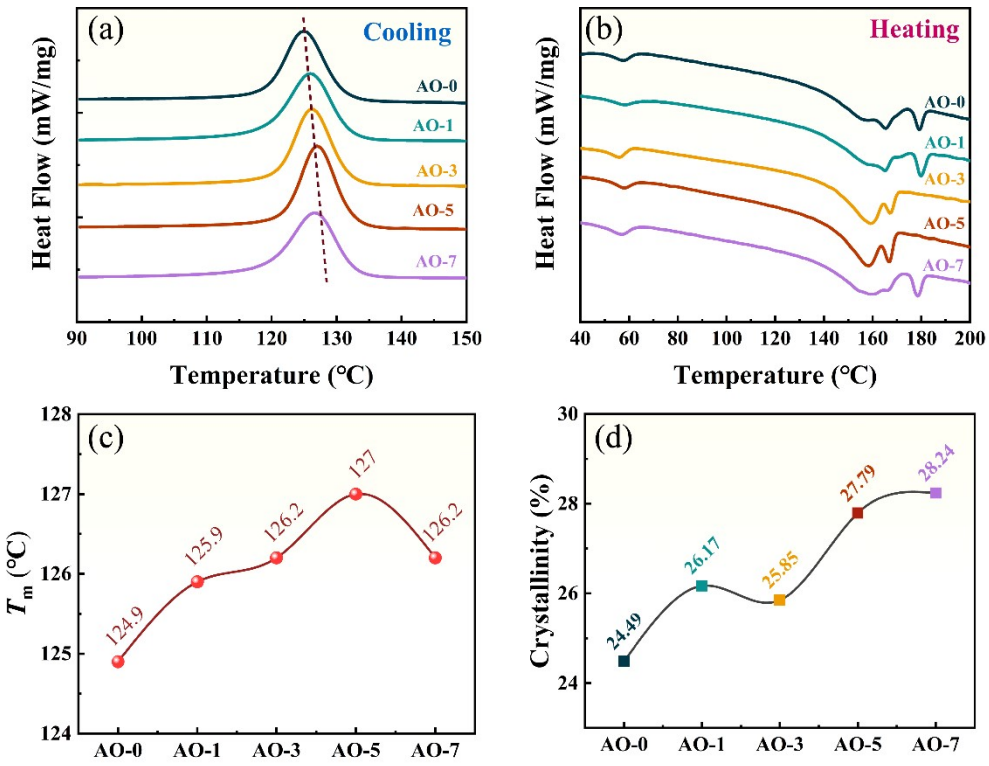

Figure S5 The DSC cooling **(a)** and **(b)** heating process of AO-x middle layer, **(c)** the T_c for AO-x middle layer and **(d)** the crystallinity of AO-x middle layer.

Table S2 ΔH_{exp} and crystallinity PMMA/PVDF blended composites with different AO contents.

AO (wt%)	ΔH_{exp} (J/g)	Crystallinity (%)
0	25.96	24.79%
1	27.40	26.17%
3	27.07	25.85%
5	29.10	27.79%
7	29.57	28.24%

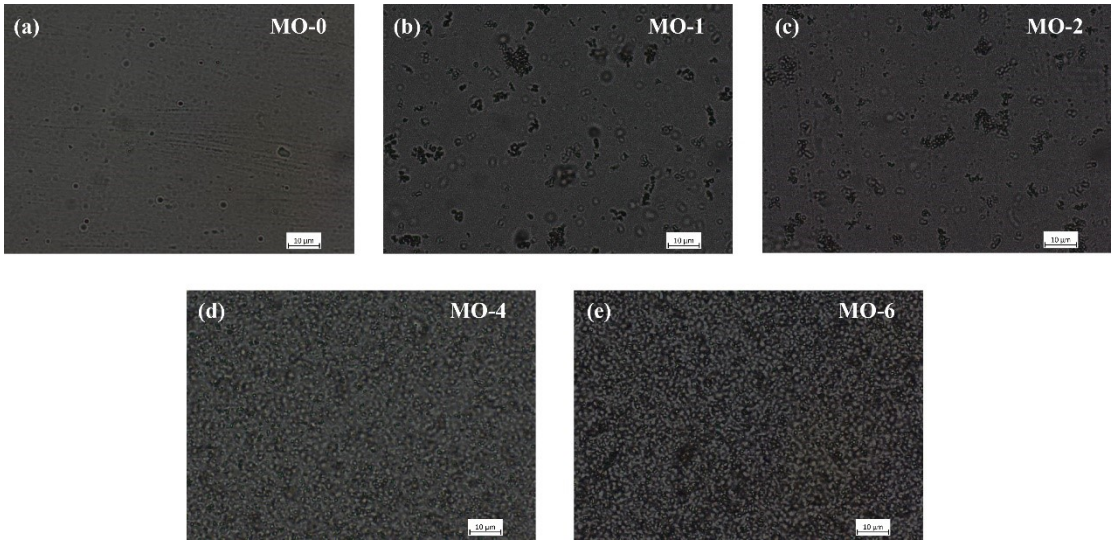

Figure S6 Spherulitic structure of **(a)** MO-0, **(b)** MO-1 **(c)** MO-2, **(d)** MO-4 and **(e)** MO-6

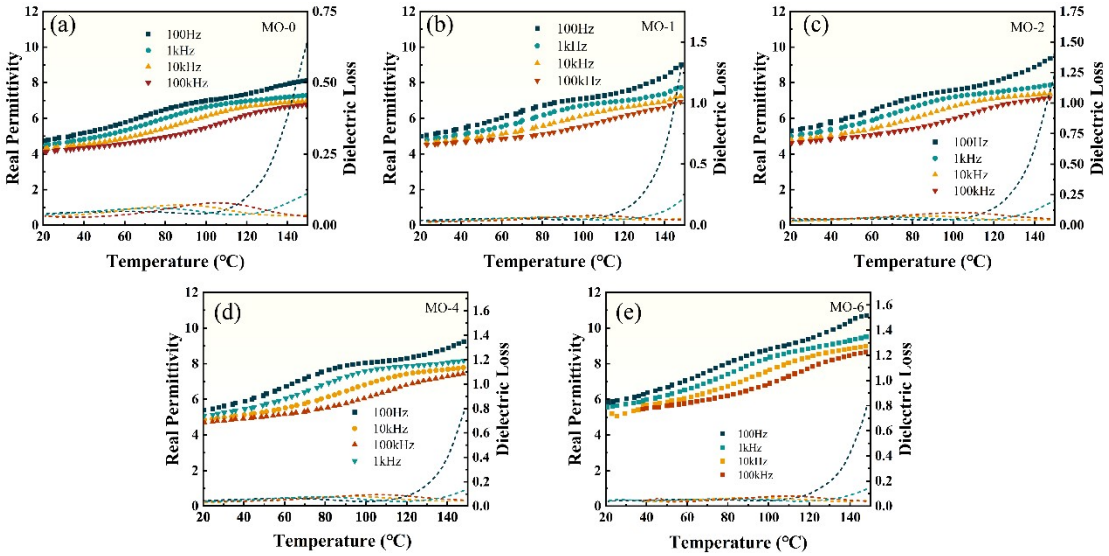

Figure S7 The permittivity and dielectric loss of **(a)** MO-0, **(b)** MO-1 **(c)** MO-2, **(d)** MO-4 and **(e)** MO-6 at various frequency as a function of temperature.

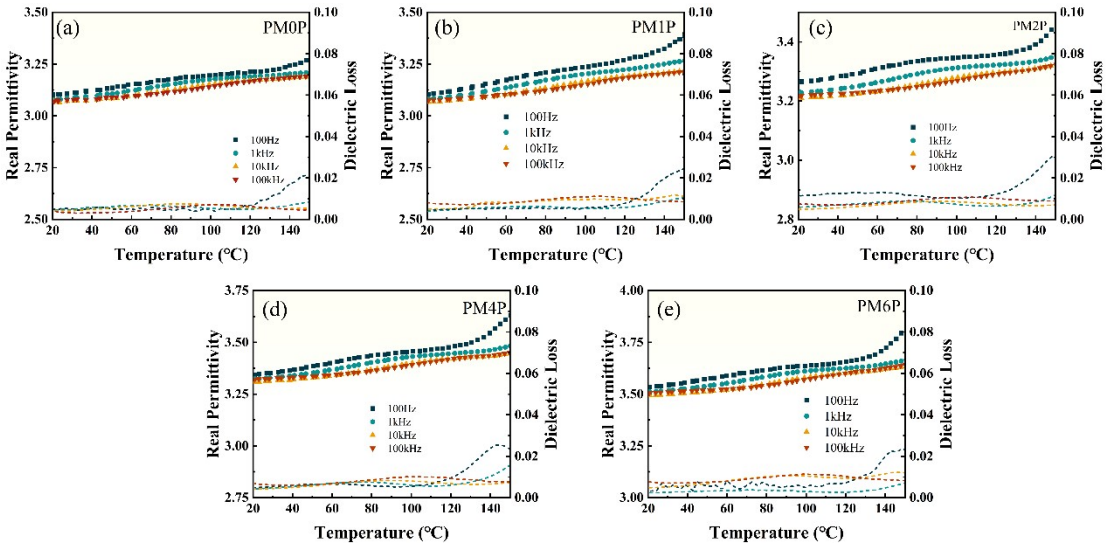

Figure S8 The permittivity and dielectric loss of **(a)** PM0P, **(b)** PM1P **(c)** PM2P, **(d)** PM4P and **(e)** PM6P at various frequency as a function of temperature.

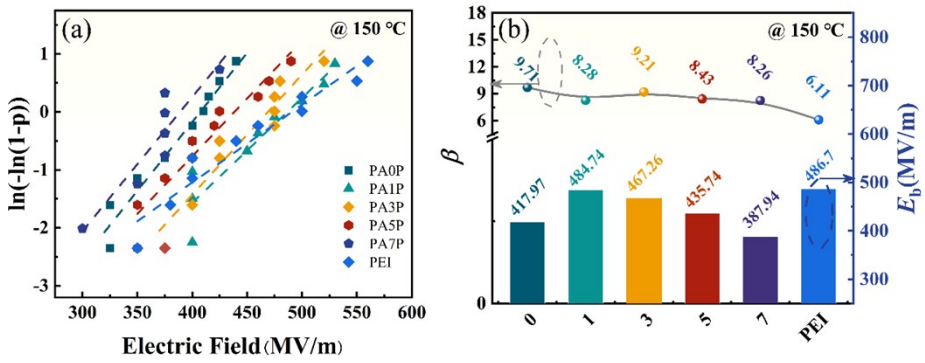

Figure S9 (a) Two-parameter Weibull distribution plots, **(b)** breakdown strength E_b and shape parameter β for PAxP

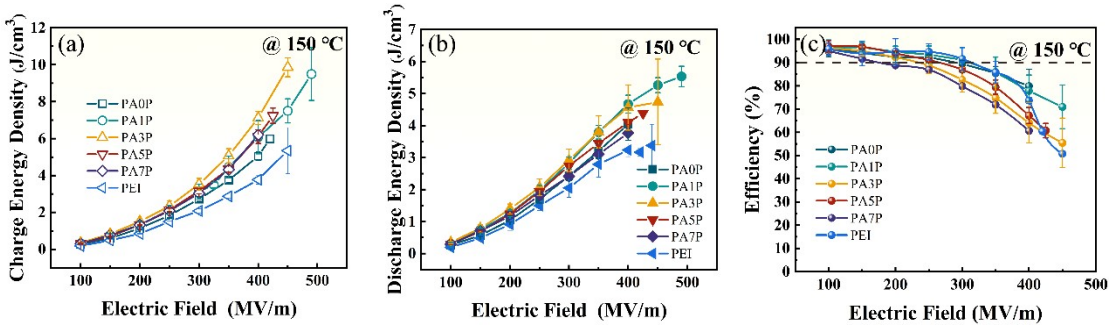

Figure S10 (a) The charge energy density, (b) the discharge energy density and (c) the efficiency of PAxP at 150 ℃.

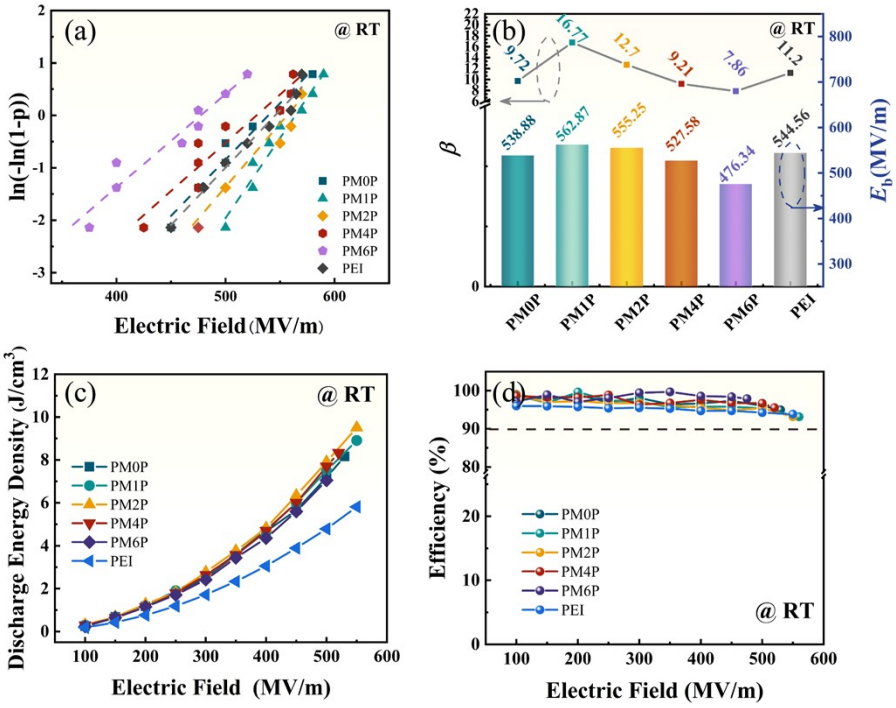

Figure S11 (a) Two-parameter Weibull distribution plots, **(b)** breakdown strength E_b and shape parameter β **(c)** discharge energy density U_d and **(d)** charge-discharge efficiency η for PMxP at RT.

At RT, all the PMxP sandwich-structured composites performs high E_b, with the MgO nps content increase in PMMA/PVDF middle layer, the E_b of composites rises up and get the highest E_b at 562.87 MV/m for PM1P. Then E_b goes down to 476.34 MV/m for PM6P, as shown in **Figure S11 (a)** and **(b)**.

The U_d and η for PMxP at RT are depicted in **Figure S11 (c)** and **(d)**, the U_d of all the sandwich-structured composites show obvious improvement compared with pure PEI, which is owing to the inserting and optimizing of MgO-PMMA/PVDF middle layer. Also, all the composites show high η greater than 90%. Eventually, The PM2P performs the highest U_d at RT, which is as high as 9.50 J/cm^3.

The applied electric field on each layer was calculated according to the series model of three capacitors, the equation is

$$\varepsilon_1 E_1 = \varepsilon_2 E_2 \tag{S3}$$

in the PMxP, the upper and lower layers of the sandwich-structured composites are both PEI, and these two layers have the same thickness, so the **Eq. (S3)** can be replaced by [S3, S4]

$$E_i = \frac{V}{d_i + 2\frac{\varepsilon_i}{\varepsilon_o} d_o} \qquad E_o = \frac{V}{2d_o + \frac{\varepsilon_o}{\varepsilon_i} d_i} \tag{S4}$$

where V is the applied voltage on the entire film, E_o is the electric field borne by the PEI layer, and E_i is the electric field borne by the middle layer. d_o, ε_o are the thickness and permittivity of the PEI layer, d_i, ε_i are that for the middle layer. According to the permittivity and thickness of each layer, the electric field applied to the middle and outer layers was calculated when the applied electric field was 300 MV/m, the results are displayed in **Figure S12**.

The middle layer permittivity increases with MgO introduction, which leads to the electric field undertaken by the PEI layer raise up, as shown in **Figure S12** and **Figure S13**, resulting in premature breakdown of the material. Therefore, with the combined influence of these factors, PM1P obtains the optimal value E_b.

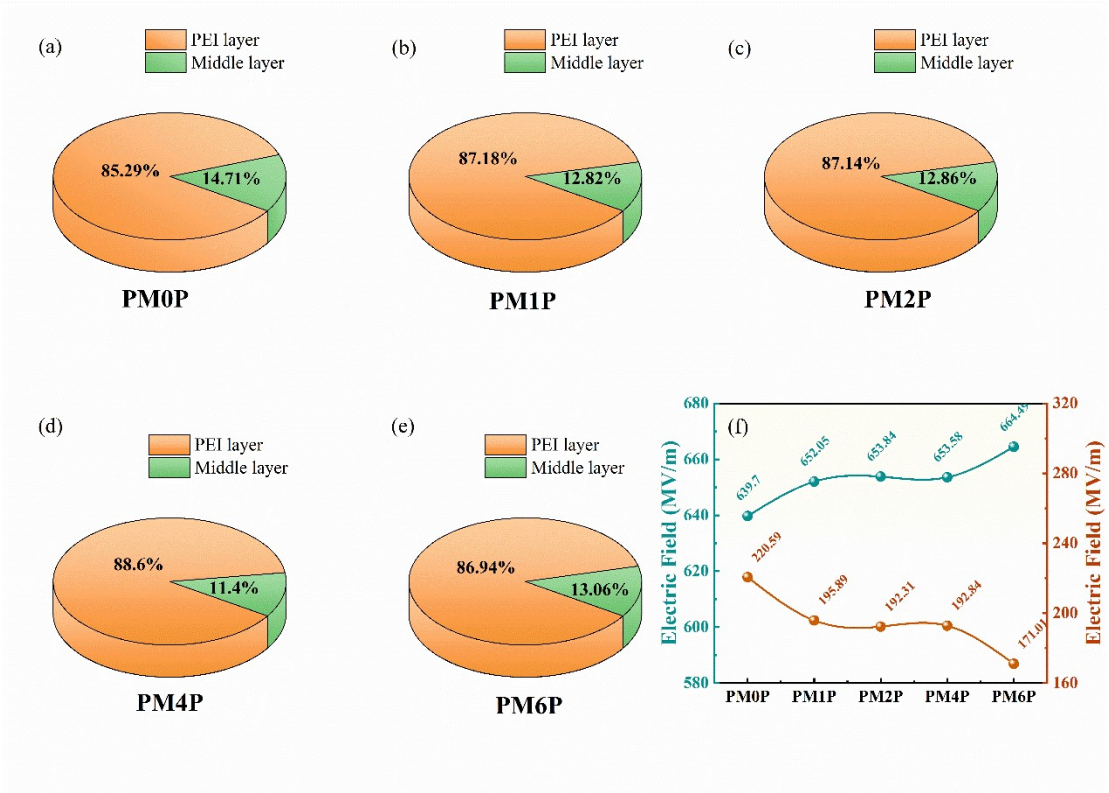

Figure S12 (a-e) The electric field distribution at 300MV/m and 150 ℃ in the PMxP sandwich-structure composites calculated according to the series capacitor model. **(f)** Variation of electric field distribution in PMxP composites as a function of MgO content in the middle PMMA/PVDF blend composite layer calculated using a series capacitor model

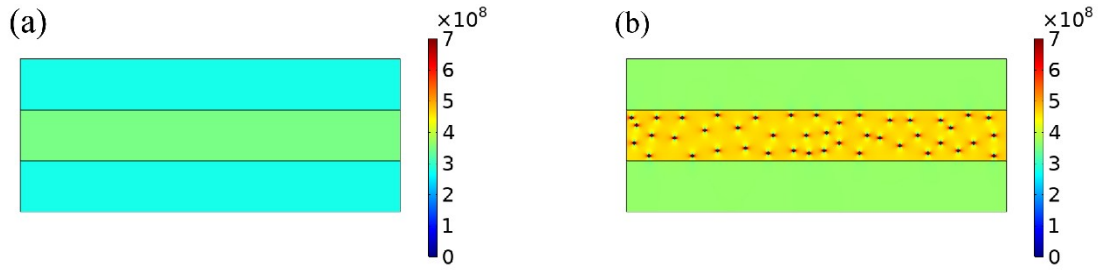

Figure S13 The electric field distribution of **(a)** PM0P and **(b)** PM1P at 150 ℃ when charging 300MV/m by finite element simulation.

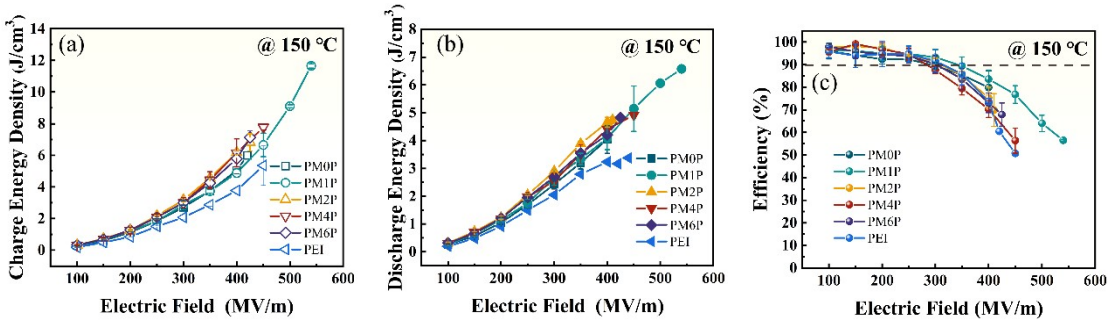

Figure S14 (a) The charge energy density **(b)** discharge energy density and **(c)** efficiency of PMxP at 150 °C.

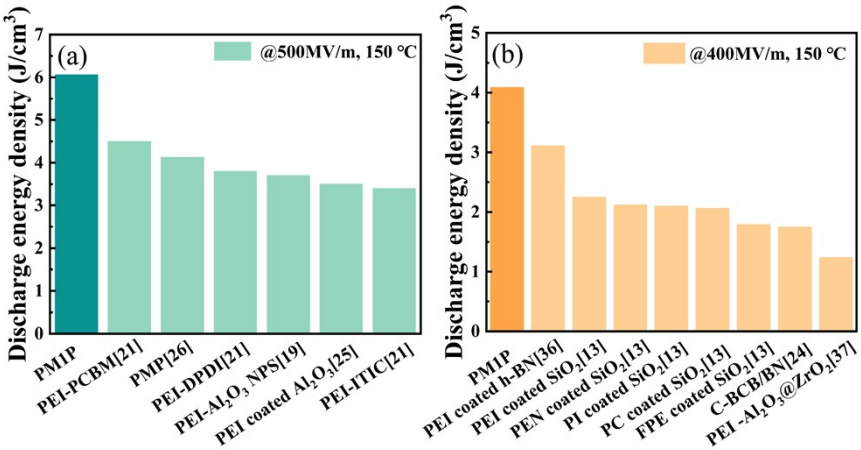

Figure S15 The comparison diagram of discharge energy density U_d at 150 °C and high electrical field (a) 500 MV/m and (b) 400MV/m for PM1P and previously reported works[13, 19, 21, 24-26, 36-38, 40].

Reference:

S1. A. S. Elmezayyen, F. M. Reicha, I. M. El-Sherbiny, J. Zheng and C. Xu, European Polymer Journal, 2017, 90, 195-208.

S2. V. Sencadas, P. Martins, A. Pitaes, M. Benelmekki, J.L. Gomez Ribelles,S. Lanceros-Mendez, , Langmuir. 27(11) (2011) 7241-7249.

S3. L. Sun, Z. Shi, B. He, H. Wang, S. Liu, M. Huang, J. Shi, D. Dastan and H. Wang, Advanced Functional Materials, 2021, 31,35, 2100280.

S4. C. Wang, G. He, S. Chen, H. Luo, Y. Yang and D. Zhang, Journal of Materials Chemistry A, 2022, 10, 9103-9113.